Supporting Information

Inman et al. 10.1073/pnas.1714058114

SI Materials and Methods

Participants. Fourteen participants with drug-resistant epilepsy volunteered to participate in the study following an invitation during their intracranial monitoring (ICM) visit that included an explanation of the possible risks and benefits (for details, see Tables S1–S3). The study protocol was approved by the Emory University Institutional Review Board, and all participants provided written informed consent. To be included in the study subjects had to be English-speaking adults (>18 y, regardless of gender, race, or ethnicity) implanted with intracranial depth electrodes, including those localized to the left or right amygdala. Subjects also had to be able to understand an informed consent (comprehend potential risks and benefits) and give written and verbal informed consent to all experiments. On average, patients were monitored in the Emory University Hospital Epilepsy Monitoring Unit for 14.4 d (SD = 6.3). Before ICM, standard stereotactic EEG depth electrode arrays (Ad-Tech; 0.86 mm diameter, 2 mm length platinum-coated contacts, typically spaced along 5-mm intervals) were implanted into the brain parenchyma by a neurosurgeon (J.T.W. or R.E.G.) for the sole purpose of clinical seizure investigation. All 14 patients had electrode contacts localized near the BLA. Five of the 14 patients also had electrode contacts localized in both the hippocampus and perirhinal cortex (see Fig. S2 and Table S2, and *Electrophysiological Data Analysis* below). The impedance of the electrodes was between 0.3 and 1 kΩ when implanted. The number of patients was predetermined by a formal power (target = 0.8) analysis that estimated the effect size of the main stimulation vs. no-stimulation memory effect based on effect sizes ranging from 0.88 to 1.02 (Cohen's d) in three prior rat studies (mean Cohen's $d = 0.95$; G*Power) (1).

Brain Stimulation and Recording.

Prospective stimulation electrode localization. High-resolution presurgical and postimplantation anatomical scans were gathered on each patient [T1 MPRAGE, Siemens 1.5T, repetition time (TR) = 1,900, echo time (TE) = 3.5]. We applied the following method to localize the precise position of the stimulating electrode contacts relative to the BLA using custom MATLAB scripts (Fig. 1 and Fig. S3). Preoperative and postoperative T1 images were aligned with an automated linear coregistration using the FLIRT module of FMRIB Software Library (FSL) (2), which was then corrected for postsurgical tissue displacement and deformation using a manually guided nonlinear thin-plate spline warping (3, 4). Control points for the nonlinear warping were selected at locations where the anatomical correspondence between pre- and postoperative images could be unambiguously identified in a side-by-side visual comparison, with emphasis on features bounding the electrode location as closely as imaging artifacts allowed. Amygdala nuclei were then projected into the space of the preoperative image through nonlinear warping of deformable meshes representing the structures of interest. The meshes were obtained by digitizing a stereotactic atlas of the human brain (5, 6) and were projected into the preoperative image space by first aligning the outer boundary of the atlas-derived amygdala with an amygdala boundary surface obtained through automated subcortical segmentation (FSL FIRST) (7), with manual adjustment of the latter to improve accuracy when necessary. These respective surfaces then provided control points for a nonlinear thin-plate spline warping, which allowed the atlas-derived meshes to be projected into the space of the subject's preoperative image. For most patients ($n = 12$) these steps were completed prospectively to aid in targeting the BLA.

Retrospective stimulation and recording electrode localization. Locations of stimulating and recording electrodes in the amygdala, hippocampus, and perirhinal cortex were verified in each patient. Electrode contacts locations were determined by automated coregistration of each postoperative structural brain T1 MRI and head computed tomography (CT) images with each preoperative brain MRI using a stereotactic neurosurgical planning computer workstation (ROSA Surgical Planning Software; MedTech Surgical, Inc.). A neurosurgeon (J.T.W.) directly compared contact locations with standard MRI and tissue-section atlases of the human brain (5, 8). Prior prospective BLA localizations were consistent with this direct retrospective method. Five subjects in whom contacts were simultaneously located in gray matter of BLA, hippocampus, and perirhinal cortex were identified, and only in these subjects were the relevant contacts utilized for further LFP record analysis (Fig. S2).

Stimulation parameters and LFP recording. Stimulation parameters were chosen to replicate those used in three prior rat studies that demonstrated amygdala-mediated memory enhancement (9–11). Specifically, stimulation was delivered to the BLA in current-regulated, charge-balanced, biphasic rectangular pulses at 0.5 mA for 1 s in eight trains of four pulses at 50 Hz. A research neurostimulator (CereStim M96; Blackrock Microsystems) was used to deliver stimulation precisely at the offset of image presentation for a randomized half of the studied images. The current, duration, and pulse frequency are well below typical clinical stimulation mapping parameters. During all sessions, a neurologist or neurosurgeon was present to monitor the subject and view the real-time LFP signals for afterdischarges and clinical seizure activity. Implanted electrodes were recorded continuously for clinical monitoring of seizure and interictal activity. No seizure activity or afterdischarges to stimulation were detected during testing or in a thorough posttest review of all recorded LFP channels by a clinical epileptologist (R.E.F.) (Table S2). LFP data from all electrodes recorded during experimental testing were clipped from the clinical file and deidentified. Sampling frequency was either 500 or 1,000 Hz. The recording voltage range was direct current to 20 mV (XLTEK EMU 128FS; Natus Medical). An extracranial subdermal electrode array at vertex was used as the common-mode ground. Computer-generated electrical pulses were recorded along with the electrophysiological data on an open channel not used for recording brain activity to allow precise synchronization of the stimuli with the neural responses.

Analysis of Memory Performance. Behavioral data were analyzed with SPSS 23 (IBM). Recognition-memory performance was calculated using estimates of the strength of the signal (endorsed repeated objects) relative to the noise (endorsed new object) (d′) (12). The d′ was calculated for each experimental condition (stimulation vs. no stimulation), and a planned paired-samples t test (two sided) was conducted for each recognition-memory test (immediate and 1-d). A 2 × 2 repeated-measures ANOVA with the factors of stimulation and test delay was also conducted to test for omnibus main effects and interactions. All data were normally distributed based on a Kolmogorov–Smirnov test of normality, and a Grubbs test (13) for each stimulation condition did not identify outliers in either test condition. To further determine the effects of post-presentation stimulation on the subsequent image (Fig. S3), we contrasted the main amygdala-mediated memory-enhancement effect with the memory performance for no-stimulation trials that occurred after a stimulation trial.

Autonomic Response to Stimulation Parameter Task. To determine safety and efficacy, an independent group of epilepsy patients (n = 7) undergoing intracranial monitoring for seizure-onset localization participated in examination of autonomic responses to a wide range of amygdala-stimulation parameters. These included screening at higher amplitudes and longer durations than those ultimately selected for memory testing. Electrodermal activity (EDA) and heart rate (electrocardiography) were continuously recorded as stimulation to the BLA was delivered at various voltage and frequency settings for 30-s periods with at least 30 s off between trials (Fig. S4). Sham stimulation control trials were randomly interspersed among actual stimulation trials. Stimulation was delivered using a voltage-controlled hand-held clinical neurostimulator (Model 3628 Dual Screen; Medtronic, Inc.). To compare screening stimulation voltages with the present study's constant amperage, we estimated the stimulation amperage given the typical range of depth electrode impedances and the neurostimulator voltages. Voltage ranged from 0.5–10 V, and frequencies ranged from 50–130 Hz. Estimating a range of impedances from 0.3–4 kΩ in our stimulation electrodes, a range well beyond the typical impedances of operational recording electrodes, stimulation at 0.5 mA would be equivalent to stimulation voltages from 0.25–2 V. Thus, for the present study, we analyzed psychophysiology data from a matched range of amplitudes (sham vs. 2 V or less at 50 Hz) used for stimulation during the recognition-memory task. Patients were asked to rest quietly during each stimulation trial, and data from any trials with vocalization artifacts were removed. Data were recorded and analyzed in AcqKnowledge 4.2 with a MP150 amplifier and wireless BioNomadix transceivers (Biopac, Inc.). EDA amplitude (square-root transformed to correct for known skew in EDA distributions) was calculated as the magnitude of the peak-to-peak change in EDA from stimulation onset to offset. Heart rate was calculated for each condition by subtracting the average heart rate (beats/min) 15 s prestimulation from the average heart rate during the 30 s of stimulation.

Electrophysiological Data Analysis.

Overview and data preprocessing. Analyses of electrophysiological data focused on oscillations in LFPs recorded simultaneously from the BLA, hippocampus, and perirhinal cortex in five patients with electrodes simultaneously present in all three regions (see Fig. S2 and previous *Brain Stimulation and Recording* section). The main question of interest was whether, on either test, oscillatory activity in the LFPs would differ between accurately recognized objects in the stimulation condition vs. the no-stimulation condition. Data from the first 0.5 s of each correctly answered trial of both the immediate and one-day memory tests were analyzed to minimize differences in test responses between participants in terms of both timing and accuracy. Analyses focused on the test sessions because electrical stimulation was delivered during the study session only after object images were presented and because the electrical stimulation produced substantial electrical artifacts in the recording channels and volume conduction effects in nearby channels. In addition, for several of the five patients in the LFP analyses, there were relatively few incorrect images in the stimulation condition on either test. Thus, comparing LFPs between correct and incorrect trials was not feasible.

Analyses of LFP data were conducted with MATLAB (MathWorks). The data were first digitally filtered with a low-pass cutoff of 1 Hz to attenuate low-frequency artifacts (the high-pass cutoff was 249 Hz). To attenuate possible 60-Hz electromagnetic noise in the LFPs, a 60-Hz sine wave was fit to each 1.5 s of data and then subtracted, impacting a narrow frequency range from ~59.5 to 60.5 Hz. The median LFP across all available recording electrodes (up to 128 for each session) was then subtracted from each LFP to remove nonlocal artifacts.

Power and coherence. Analyses of oscillations were assisted by an open-source library of functions (chronux.org) that implemented a multitaper fast Fourier transform (FFT) method for calculating spectral power and coherence, which reduces variance and bias compared with standard FFT analyses (14). A frequency bandwidth of ±10 Hz, which permitted nine orthogonal tapers for the 0.5-s data, was used for frequency ranges above 15 Hz, but a frequency bandwidth of ±6 Hz (with five tapers) was used for lower ranges due to the narrower frequency peaks of theta oscillations. To permit valid statistical comparisons between conditions, coherence estimates were Fisher Z transformed, power estimates were log10 transformed (and multiplied by 10 to convert from bels to decibels), and both were corrected for bias as described previously (15). Power and coherence estimates for a 0.5-s pretrial baseline period (just before image onset) were calculated and subtracted from the respective estimates for the test trial period to remove possible nonspecific fluctuations in the data. To evaluate statistical significance between stimulation and no-stimulation conditions, mean power and coherence values in both conditions were calculated for each participant for the theta (5–7 Hz) and gamma (30–55 Hz, sometimes termed "slow gamma") ranges based on the prominence of these ranges in past studies of recognition memory across rats, monkeys, and humans (16–19). The mean values for each patient in each range in the stimulation and no-stimulation conditions were then compared using a paired t test. Bonferroni corrections for multiple comparisons were applied for the six paired t tests performed for each memory test for power and coherence to maintain an overall $\alpha = 0.05$. Under this correction, the effect of prior amygdala stimulation on perirhinal gamma power, but not the perirhinal–hippocampal theta coherence effect, would survive this conservative alpha correction of 0.05/6.

Theta–gamma comodulation analyses. To calculate the extent to which the amplitude of gamma oscillations in perirhinal cortex were related to the phase of theta oscillations in the BLA, a phase–amplitude modulation index (MI) was calculated for the first 0.5 s of each test trial as described previously (20, 21). Briefly, LFPs from the BLA were first band-pass filtered for the theta range. The amplitude of perirhinal oscillations from 20–100 Hz (in 20-Hz frequency bins stepped at 5-Hz intervals) was then estimated (using the amplitude of the complex Hilbert transform) for each 20° bin (1/18th) of the theta phase. The degree to which the amplitude of the higher oscillations varied across theta-phase bins was then estimated by quantifying (using a normalized Kullback–Leibler distance) how the observed distribution differed from a uniform distribution. The resulting MI values could have ranged from 0 (i.e., no modulation of higher-frequency amplitudes by theta phase) to 1 (perfect modulation). To evaluate statistical significance between stimulation and no-stimulation conditions for both tests, MI values for the no-stimulation condition were subtracted from the MI values for stimulation condition. The mean MI difference in the gamma (30–55 Hz) range for each of the five patients used in LFP analyses was then compared with 0 using a one-sample t test for both the immediate and one-day tests.

1. Faul F, Erdfelder E, Lang A-G, Buchner A (2007) G*Power 3: A flexible statistical power analysis program for the social, behavioral, and biomedical sciences. *Behav Res Methods* 39:175–191.
2. Jenkinson M, Smith S (2001) A global optimisation method for robust affine registration of brain images. *Med Image Anal* 5:143–156.
3. Bookstein FL (1989) Principal warps: Thin-plate splines and the decomposition of deformations. *IEEE Trans Pattern Anal Mach Intell* 11:567–585.
4. Rohr K, et al. (2001) Landmark-based elastic registration using approximating thin-plate splines. *IEEE Trans Med Imaging* 20:526–534.
5. Mai JK, Paxinos G, Voss T (2007) *Atlas of the Human Brain* (Academic, Cambridge, MA), 3rd Ed.
6. Oya H, Kawasaki H, Dahdaleh NS, Wemmie JA, Howard MA, 3rd (2009) Stereotactic atlas-based depth electrode localization in the human amygdala. *Stereotact Funct Neurosurg* 87:219–228.

7. Patenaude B, Smith SM, Kennedy DN, Jenkinson M (2011) A Bayesian model of shape and appearance for subcortical brain segmentation. *Neuroimage* 56:907–922.
8. Duvernoy H (2005) *The Human Hippocampus* (Springer, Berlin).
9. Bass DI, Manns JR (2015) Memory-enhancing amygdala stimulation elicits gamma synchrony in the hippocampus. *Behav Neurosci* 129:244–256.
10. Bass DI, Nizam ZG, Partain KN, Wang A, Manns JR (2014) Amygdala-mediated enhancement of memory for specific events depends on the hippocampus. *Neurobiol Learn Mem* 107:37–41.
11. Bass DI, Partain KN, Manns JR (2012) Event-specific enhancement of memory via brief electrical stimulation to the basolateral complex of the amygdala in rats. *Behav Neurosci* 126:204–208.
12. Macmillan NA, Kaplan HL (1985) Detection theory analysis of group data: Estimating sensitivity from average hit and false-alarm rates. *Psychol Bull* 98:185–199.
13. Grubbs FE (1950) Sample criteria for testing outlying observations. *Ann Math Stat* 21:27–58.
14. Bokil H, Andrews P, Kulkarni JE, Mehta S, Mitra PP (2010) Chronux: A platform for analyzing neural signals. *J Neurosci Methods* 192:146–151.
15. Bokil H, Purpura K, Schoffelen J-M, Thomson D, Mitra P (2007) Comparing spectra and coherences for groups of unequal size. *J Neurosci Methods* 159:337–345.
16. Fell J, et al. (2001) Human memory formation is accompanied by rhinal-hippocampal coupling and decoupling. *Nat Neurosci* 4:1259–1264.
17. Trimper JB, Stefanescu RA, Manns JR (2014) Recognition memory and theta-gamma interactions in the hippocampus. *Hippocampus* 24:341–353.
18. Jutras MJ, Fries P, Buffalo EA (2009) Gamma-band synchronization in the macaque hippocampus and memory formation. *J Neurosci* 29:12521–12531.
19. Jutras MJ, Fries P, Buffalo EA (2013) Oscillatory activity in the monkey hippocampus during visual exploration and memory formation. *Proc Natl Acad Sci USA* 110:13144–13149.
20. Tort ABL, Komorowski RW, Manns JR, Kopell NJ, Eichenbaum H (2009) Theta-gamma coupling increases during the learning of item-context associations. *Proc Natl Acad Sci USA* 106:20942–20947.
21. Tort ABL, Komorowski R, Eichenbaum H, Kopell N (2010) Measuring phase-amplitude coupling between neuronal oscillations of different frequencies. *J Neurophysiol* 104: 1195–1210.

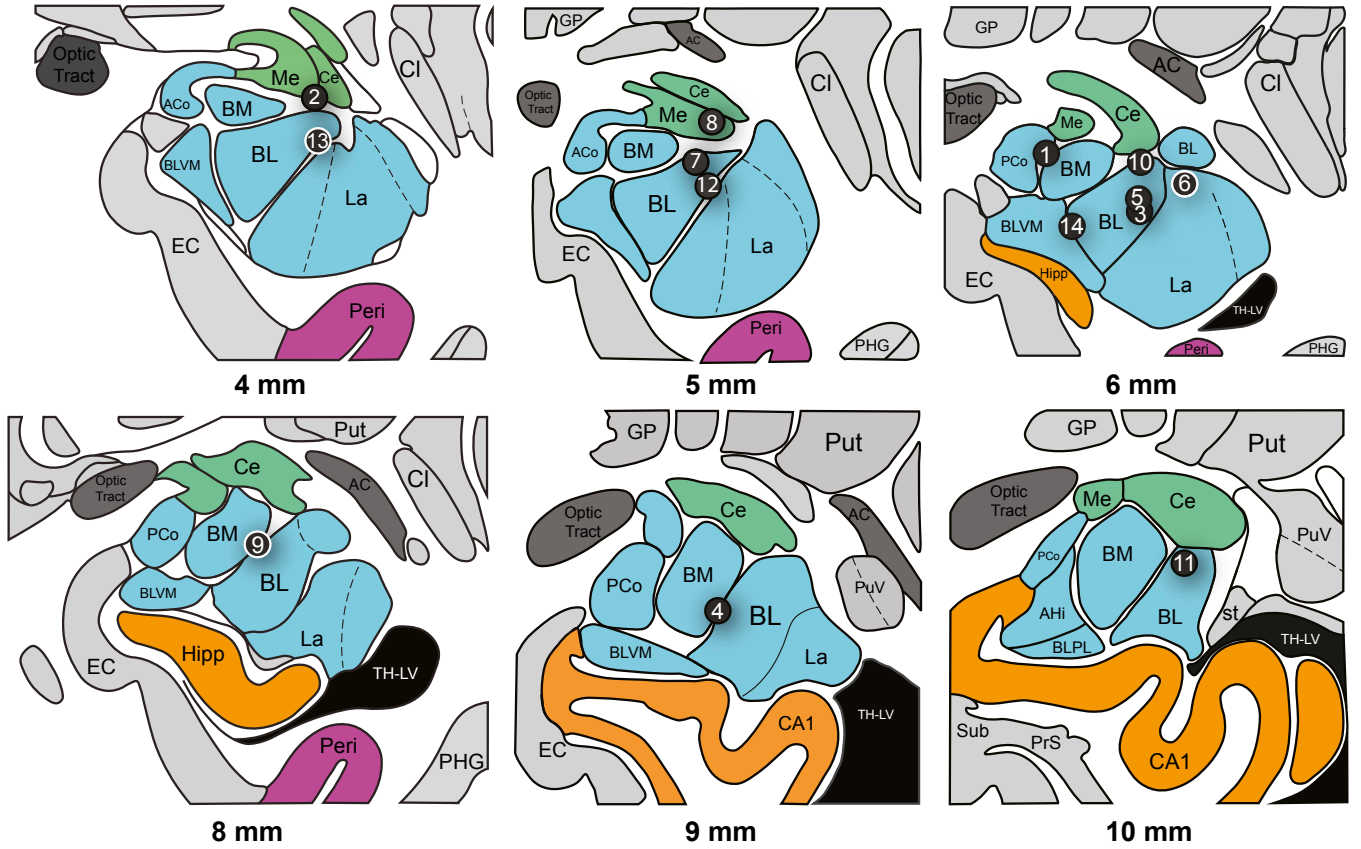

Fig. S1. Precise localization of stimulation sites overlaid on illustrated coronal slices through the human amygdala. Black circles indicate estimated centroids of bipolar stimulation in or near the BLA in all 14 patients (white borders on circles denote right-sided stimulation). Distance are given in millimeters from the anterior commissure (0,0,0) point in the anterior-to-posterior direction (*y* axis). AC, anterior commissure; ACo, anterior cortical amygdala nucleus; AHi, amygdala hippocampal area; BL, basolateral amygdala nucleus; BLA, basolateral complex of the amygdala; BLPL, basolateral nucleus, paralaminar part; BLVM, basolateral amygdala, ventromedial part; BM, basomedial nucleus; CA1, CA1 field of the hippocampus; Ce, central amygdala nucleus; Cl, claustrum; EC, entorhinal cortex; GP, globus pallidus; La, lateral amygdala nucleus; Me, medial amygdala nucleus; PCo, posterior cortical amygdala nucleus; Peri, perirhinal cortex; PHG, parahippocampal gyrus; PrS, presubiculum; Put, putamen; PuV, ventral putamen; st, stria terminalis; Sub, subiculum; TH-LV, temporal horn of the lateral ventricle. Adapted with permission from ref. 1, copyright Elsevier 2007.

1. Mai JK, Paxinos G, Voss T (2007) *Atlas of the Human Brain* (Academic, Cambridge, MA), 3rd Ed.

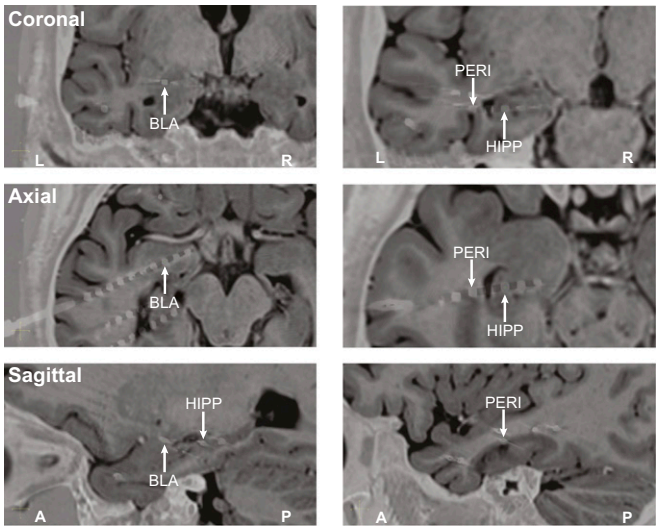

Fig. S2. Merged high-resolution preoperative MRI and postoperative CT in a representative patient demonstrates the location of LFP recording electrode contacts in the BLA, hippocampus (HIPP), and perirhinal cortex (PERI). Postoperative CT scans linearly coregistered to the coronal, axial, and sagittal planes of a patient's preoperative MRI scan. The electrodes are shown in the amygdala (BLA), hippocampal (HIPP), and perirhinal (PERI) regions in one subject (subject 8). Electrodes were localized using the Mai atlas (1) and the Duvernoy MTL atlas (2). A, anterior; L, left; P, posterior; R, right. (Magnification: 4×.)

1. Mai JK, Paxinos G, Voss T (2007) *Atlas of the Human Brain* (Academic, Cambridge, MA), 3rd Ed.
2. Duvernoy H (2005) *The Human Hippocampus* (Springer, Berlin).

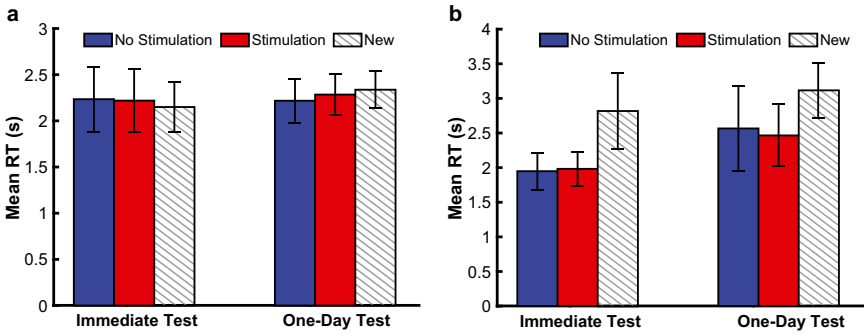

Fig. S3. Reaction times (RT) for recognition of previously viewed (red and blue bars) vs. new (hatched bar) images at the immediate and one-day recognition tests. (*A*) Prior stimulation had no significant effect on reaction time of yes/no responses during the immediate or one-day recognition test. (*B*) Prior stimulation had no significant effect on the reaction times of "yes" responses during the immediate or one-day recognition test. Patients' response times were longer on average for "yes" responses to new items at the immediate test (i.e., false alarms). These results suggest that amygdala-mediated memory enhancement did not produce reduced reaction times in subsequent testing. Error bars represent the SEM.

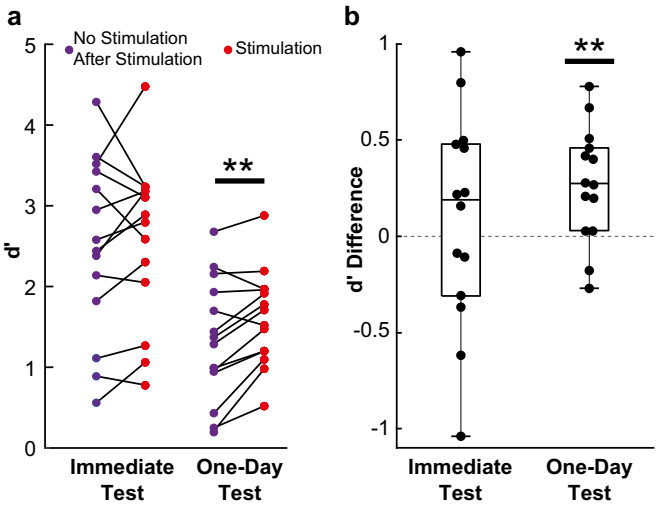

Fig. S4. Recognition-memory performance for objects followed by stimulation relative to no-stimulation objects that came after stimulation for each patient. (*A*) Recognition-memory performance (stimulation trials − no-stimulation trials after stimulation trials) for each patient plotted as a discriminability index (d′). (*B*) Recognition-memory test performance for each patient was plotted as the difference in d′ between the stimulation and no-stimulation-after-stimulation objects [t (13) = 3.4, $P = 0.005$, Cohen's $d = 0.91$]. If stimulation enhanced memory for subsequent nonstimulated items, then the data would show a decrease of our original memory-enhancement effect across patients, but if stimulation diminished memory for subsequent nonstimulated items, then the data would show an increase of our original memory-enhancement effect across patients. These results suggest no evidence of a change in our original effect and thus no significant carry-over (i.e., order) effect of episodes of stimulation upon the subsequent object-encoding trials. $^{**}P < 0.005$.

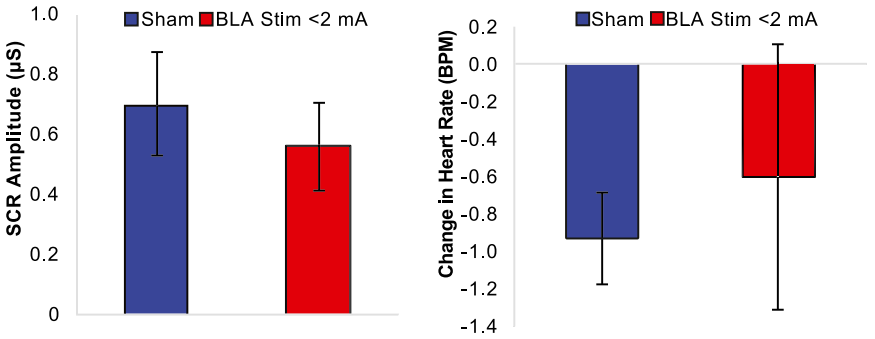

Fig. S5. No evident autonomic effects of BLA stimulation were seen in a separate parameter sweep experiment with similar stimulation parameters. During a separate stimulation parameter sweep experiment ($n = 7$ subjects), no effect of BLA stimulation on the magnitude of the skin conductance response (SCR) or changes in heart rate in beats/min (BPM) at <2 mA was seen relative to a sham condition. Stimulation or sham stimulation was delivered for 30 s on and 30 s off at 50 Hz and a pulse width of 300 μs.

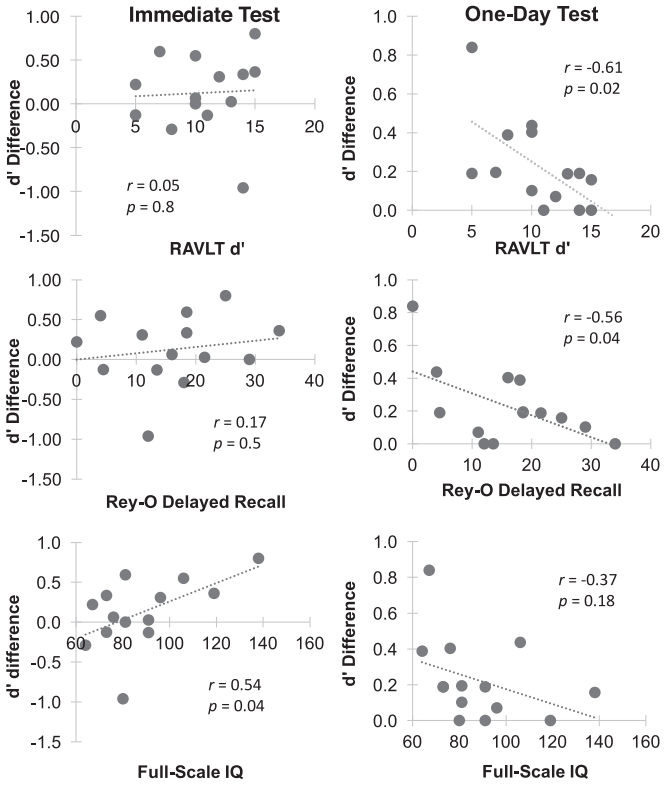

Fig. S6. Correlations between the amygdala-mediated memory-enhancement effect at the one-day test and baseline memory and cognitive capacity. The Rey–Osterrieth (Rey-O) Delayed Recall and Rey Auditory Verbal Learning Test (RAVLT) were selected because they relate most directly to the delayed visual recognition memory used in the study.

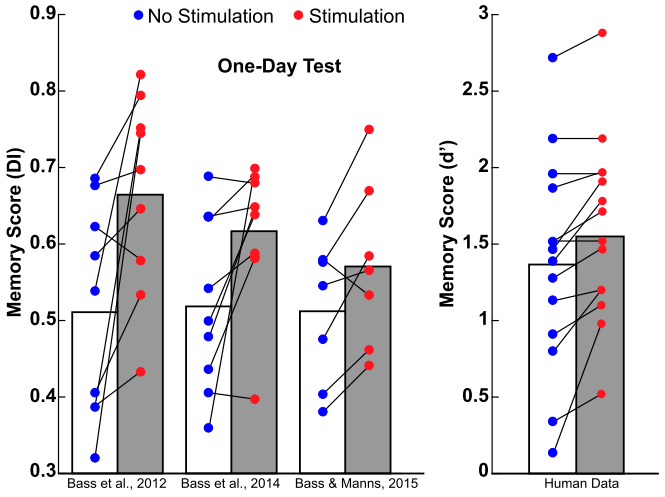

Fig. S7. Discrimination index (DI) between objects followed by stimulation vs. no stimulation during the one-day test in three analogous studies in rats (1–3) and the present study in humans. Rat study results: $P = 0.02$, Cohen's $d = 0.95$ (1); $P = 0.03$, Cohen's $d = 0.88$ (2); and $P = 0.04$, Cohen's $d = 1.02$ (3). Human study: $P = 0.003$, Cohen's $d = 0.98$. The discrimination index (DI) is derived from the ratio of the time in which a rat explores repeated vs. new objects. A DI of 0.5 represents no memory or equal exploration of the repeated and new objects. A DI greater than 0.5 represents better memory for repeated objects in a specific condition.

1. Bass DI, Partain KN, Manns JR (2012) Event-specific enhancement of memory via brief electrical stimulation to the basolateral complex of the amygdala in rats. *Behav Neurosci* 126: 204–208.
2. Bass DI, Nizam ZG, Partain KN, Wang A, Manns JR (2014) Amygdala-mediated enhancement of memory for specific events depends on the hippocampus. *Neurobiol Learn Mem* 107: 37–41.
3. Bass DI, Manns JR (2015) Memory-enhancing amygdala stimulation elicits gamma synchrony in the hippocampus. *Behav Neurosci* 129:244–256.

Table S1. Participant demographics and relevant neuropsychological testing scores

Subject	Sex	Age, y	Language dominance	FSIQ	VCI	PRI	RAVLT total	RAVLT d′	Rey-O delayed
1	M	54	Unknown	73	76	81	22	5	4.5
2	F	20	L	81	80	94	44	10	29
3	M	22	L	76	76	75	51	10	16
4	M	25	R	80	89	86	58	14	12
5	F	40	Unknown	67	80	69	22	5	0
6	M	26	L	119	122	121	60	15	34
7	F	48	B/l	138	127	127	58	15	25
8	F	21	L	96	103	92	48	12	11
9	M	47	B/l	73	78	90	42	14	18.5
10	M	53	R	106	125	98	58	10	4
11	M	36	L	91	103	88	42	11	13.5
12	M	38	L	91	80	111	38	13	21.5
13	M	45	L	64	74	77	37	8	18
14	F	22	Unknown	81	93	90	34	7	18.5

All subjects reported being right hand-dominant. Hemisphere of language dominance is unknown for some participants because their functional MRI or intracarotid sodium amobarbital procedure (i.e., Wada test) results were inconclusive. RAVLT total score is out of 75; Rey-O delayed score is out of 36.B/l, bilateral; FSIQ, Full-Scale Intelligence Quotient; L, left; PRI, Perceptual Reasoning Index; R, right; RAVLT, Rey Auditory Verbal Learning Test; Rey-O, Rey–Osterrieth Complex Figure Task; VCI, Verbal Comprehension Index.

Table S2. Intracranial monitoring results

Subject	Stimulated amygdala	Interictal spike frequency	Total seizure events	Seizure day before (focal)	Between-test seizure (focal)	Determined seizure focus
1	L	+	7	0	0	L hippocampus
2	L	+	41	3	1	R supplementary motor area
3*	L	+++	2	0	0	L hippocampus
4	L	+++	53	2	1	R posterior frontal lobe
5	L	++++	7	6	0	B/l hippocampi
6*	R	+++	19	0	4	R lateral temporal lobe
7	L	+++	8	1	1	L temporal lobe
8*	L	+++	4	0	0	L hippocampus
9	R	+++	22	0	0	L parieto-temporal junction
10*	L	++	8	0	0	L hippocampus
11	L	++	8	0	2	L fronto-temporal region
12	L	+++	4	1	3	L hippocampus
13	R	—	13	2	3	L cingulum
14*	L	++	8	0	1	B/l hippocampi

Despite typical interictal epileptiform spiking activity, no patients had evoked afterdischarges or seizures during the study session. Despite the occurrence of typical focal seizures between test sessions in more than half of the patients, no patients exhibited generalized tonic–clonic seizure activity between tests. Interictal spike frequency: +, rare; ++, occasional; +++, abundant; ++++, constant. B/l, bilateral.
*Patients' data used in local field potential analysis.

Table S3. General epilepsy patient information

Subject	Seizure focus	Preoperative imaging findings	Prescribed AEDs	AEDs during testing
1	L hippocampus	R ATL; R perisylvian/parietal polymicrogyria	Lacosamide, lamotrigine	Lacosamide, lamotrigine
2	R supplementary motor area	Normal	Levetiracetam, topiramate, clorazepate, lacosamide	Levetiracetam, topiramate, clorazepate, lacosamide
3	L hippocampus	B/l temporal encephalocoeles	Clonazepam, lacosamide, lamotrigine, zonisamide	Clonazepam
4	R posterior frontal lobe	Posttraumatic R hemisphere encephalomalacia	Levetiracetam, lacosamide	Lacosamide, levetiracetam
5	B/l hippocampi	Diffuse global volume loss	Clobazam, lacosamide, lamotrigine, levetiracetam, phenytoin, pregabalin	Clobazam, lacosamide, lamotrigine, levetiracetam, phenytoin, pregabalin
6	R lateral temporal lobe	R lateral temporal resection cavity; s/p astrocytoma resection	Levetiracetam, lacosamide	Levetiracetam
7	L temporal lobe	Normal	Topiramate, pregabalin	None
8	L hippocampus	L temporal pole white matter change	Pregabalin, lamotrigine	Lamotrigine, pregabalin
9	L parieto-temporal junction	B/l perisylvian polymicrogyria	Levetiracetam, valproate, oxcarbazepine	Levetiracetam, valproate, oxcarbazepine
10	L hippocampus	Partial ATL with preserved amygdala/hippocampus	Clonazepam, gabapentin	Clonazepam
11	L fronto-temporal region	Normal	Levetiracetam, clonazepam, vigabatrin	Vigabatrin
12	L hippocampus	Normal	Lamotrigine, gabapentin, levetiracetam	Lamotrigine, gabapentin, levetiracetam
13	L cingulum	Normal	Clonazepam, carbamazepine	Carbamazepine, topiramate
14	B/l hippocampi	R anterior temporal signal abnormality	Lacosamide, zonisamide, oxcarbazepine	Lacosamide

AEDs, anti-epileptic drugs; ATL, anterior temporal lobectomy; B/l, bilateral; L, left; R, right; s/p, status post procedure.